Sub-nanometer Control of the Interlayer Spacing in Thin Films of Intercalated Rodlike Conjugated Molecules

ARTICLE *in* THE JOURNAL OF PHYSICAL CHEMISTRY B · DECEMBER 2007

Impact Factor: 3.3 · DOI: 10.1021/jp077158r · Source: PubMed

7 AUTHORS, INCLUDING:

Ingo Salzmann
Humboldt-Universität zu Berlin
82 PUBLICATIONS **1,928** CITATIONS
SEE PROFILE

Bert Nickel
Ludwig-Maximilians-University of Munich
103 PUBLICATIONS **2,498** CITATIONS
SEE PROFILE

Jürgen P. Rabe
Humboldt-Universität zu Berlin
386 PUBLICATIONS **13,360** CITATIONS
SEE PROFILE

ARTICLES

Sub-nanometer Control of the Interlayer Spacing in Thin Films of Intercalated Rodlike Conjugated Molecules

Jörn-Oliver Vogel,[†] Ingo Salzmann,[†] Ricarda Opitz,[†] Steffen Duhm,[†] Bert Nickel,[‡] Jürgen P. Rabe,[†] and Norbert Koch*[,†]

Institut für Physik, Humboldt-Universität zu Berlin, Newtonstrasse 15, D-12489 Berlin, Germany, and Department für Physik and CeNS, Ludwig-Maximilians-Universität München, D-80539 München, Germany

Received: September 6, 2007; In Final Form: October 17, 2007

Organic molecular beam co-deposition of rodlike conjugated molecules with an alkylated analogue resulted in thin film structures with layers of alternating semiconducting (conjugated molecular parts) and insulating (alkyl parts) character. By varying the alkylated molecule ratio, we could adjust the distance between conjugated layers with sub-nanometer precision, exploiting the mechanical flexibility of the alkyl chains. Furthermore, due to mutual molecular intercalation, mixed layers containing two conjugated moieties with vastly different electronic properties could be fabricated.

Introduction

The controlled fabrication of nanoscale supramolecular structures via self-assembly is a potentially advantageous route toward novel materials, since traditional "top-down" structuring methods fail on a molecular scale.[1−4] The arrangement of dissimilar molecules in a new composite material can result in physical properties that are different from just the sum of the properties of its constituents. On the other hand, being able to adjust the distance between organic conjugated molecules allows for a control of intermolecular coupling strength and thereby for influence on optical and charge transport properties. Many examples for molecular composites have been reported, mostly focusing on solution-processing[2−10] and/or structures in the monolayer range.[1−4,9,11,12] Very limited information exists on the preparation and properties of new composite materials via co-deposition of two different organic molecules from the gas phase onto a solid substrate, which offers the advantage of solvent-free processing and easy control over thin film thickness. Almost exclusively, such studies were directed at donor/acceptor molecule pairs for the application in bulk heterojunction photovoltaic cells[13−15] and light-emitting diodes.[16] Often, pronounced phase separation is observed.[17−19] However, to control or direct the self-assembly of coevaporated materials, a fundamental understanding of the mechanisms governing intercalation and phase separation for sublimed systems on the molecular scale is essential.

The present work focuses on the mechanism of mutual intercalation of rodlike and alkylated rodlike molecular materials, which have already been used to fabricate devices in the context of "Organic Electronics", i.e., α-sexithiophene (6T),[20,21] its alkylated analogue α,ω-dihexylsexithiophene (DH6T),[22−24] and *p*-sexiphenyl (6P).[24,25] Thin films of 6T, DH6T, and 6P (for chemical structures see insets in Figures 2a and 5a) evaporated onto insulating substrates typically exhibit layered structures with fiber textures.[26,27] The arrangement of molecules within one layer is mainly determined by relatively strong interactions of the molecular π-systems, whereas between the layers weaker van der Waals interactions prevail.[22] We co-deposited respective pairs of these molecular materials onto native silicon oxide and Mylar substrates (a polymeric gate insulator used in all-organic thin film transistors[28,29]) and studied structural properties of the resulting thin film samples by atomic force microscopy (AFM), X-ray diffraction (XRD), and infrared spectroscopy (IR). As a key result, we found evidence for mutual intercalation for the pairs 6T/DH6T and 6P/DH6T in thin films. Furthermore, the interlayer distance of neighboring molecular layers could be varied as a function of the molecular mixing ratio in the range of ca. 2.3 to ca. 3.7 nm, enabled by the conformational flexibility of the DH6T hexyl chains, which at the same time act as insulators between the conjugated molecular cores.

Experimental Section

Si(100) coupons (10 mm^2) covered with native oxide with a typical root-mean-square (rms) surface roughness of 0.2 nm (determined by AFM) and 1.9 μm thick Mylar sheets (DuPont; rms roughness ca. 1 nm) served as substrates. 6T (Aldrich) was purified prior to use by vacuum sublimation, DH6T (H. C. Starck GmbH) was purchased highly purified from the manufacturer, and 6P (TCI Europe) was used as received. Thin films of the organic materials were fabricated by sublimation from individual resistively heated Al_2O_3 crucibles in a custom vacuum chamber (base pressure, 5×10^{-8} mbar). The constant deposition rate of the organic materials was verified before and after film fabrication with a quartz microbalance placed at the sample position. The films' nominal mass thicknesses given here were

* To whom correspondenc should be addressed. E-mail: norbert.koch@physik.hu-berlin.de. Fax: +49 30 2093 7632.
† Humboldt-Universität zu Berlin.
‡ Ludwig-Maximilians-Universität München.

10.1021/jp077158r CCC: $37.00
Published on Web 12/04/2007

obtained as the product of deposition rate and time. For co-deposition, one source was heated until it reached the desired stable deposition rate, then the second source was added, and the total rate was measured (typically 0.5 nm/min for all samples). Unless otherwise noted, only the total nominal film thickness, the 6T mass fraction (% 6T), or the 6P mass fraction (% 6P) is indicated.

Sample characterization with AFM was performed in ambient air with a Multimode Nanoscope IV (Veeco) operated in tapping mode. The software package SPIP (Image Metrology A/S) was used for image analysis. Fourier-transform infrared spectroscopy (IR) spectra were recorded at 2 cm^{-1} resolution with an IFS 66v/S (Bruker), using a midrange mercury−cadmium telluride photodetector (MCT) detector and ratioed against spectra of the bare substrates. Transmission geometry with normal beam incidence was used, and 1000 scans were averaged. X-ray reflectivity experiments were conducted at the synchrotron light source Hasylab (Hamburg, Germany), at beamline W1. All sample preparation steps and measurements were performed at room temperature.

Results and Discussion

First, we discuss the results for co-deposited thin films of 6T and DH6T, for which the conjugated molecular moiety is identical. Representative AFM images of pure 6T and DH6T, as well as of co-deposited 6T/DH6T films of 20 nm nominal thickness, are depicted in Figure 1. For pure DH6T (0% 6T; Figure 1a), islands exhibiting three distinct height levels can be seen. Some islands were interconnected and exhibited a "liquid-like" appearance. A rather similar morphology was observed for 17% 6T (not shown), however, with smaller and less interconnected islands. The 57% 6T film (Figure 1b) exhibited a more granular appearance with less round island shapes compared to Figure 1a. The morphology of the 78% 6T film (Figure 1c) displays more pyramidlike islands, with more apparent height levels of individual terraces. Finally, pure 6T (Figure 1d) also showed the characteristic pyramidlike morphology with at least seven exposed molecular layers, however, with reduced island density and heavily fringed island edges. Films of 40−50 nm nominal thickness had very similar morphologies (not shown).

Apparently, the surface morphology changed gradually depending on the ratio between DH6T and 6T. In general, DH6T-rich films exhibited interconnected smooth-edged islands with only two to three layers forming terraces; 6T-rich films showed more pronounced fringed-island formation with more molecular layers forming the surface-exposed pyramid terraces. A detailed analysis of the AFM image height distributions allows one to asses the step height of terraces with high precision. The height distributions for all samples (insets in Figure 1) showed well-defined peaks, whose distance corresponds to the distinct step height of island terraces. (The background between peaks is attributed to the convolution of sample morphology with the AFM tip shape. The very bright spots seen in some images are attributed to surface contamination, which do not contribute to the step-height evaluation since they are higher than 10 nm.) The peaks could adequately be fitted with Gaussian distributions. To derive the average step height, the resulting peak maxima were plotted as a function of peak number, and a linear fit was applied. The results of this analysis routine are summarized in Figure 2b, together with data from additional samples not depicted in Figure 1.

In X-ray diffraction, pure DH6T films on a native silicon oxide exhibited two peaks at 0.173 and 0.345 $Å^{-1}$ of vertical

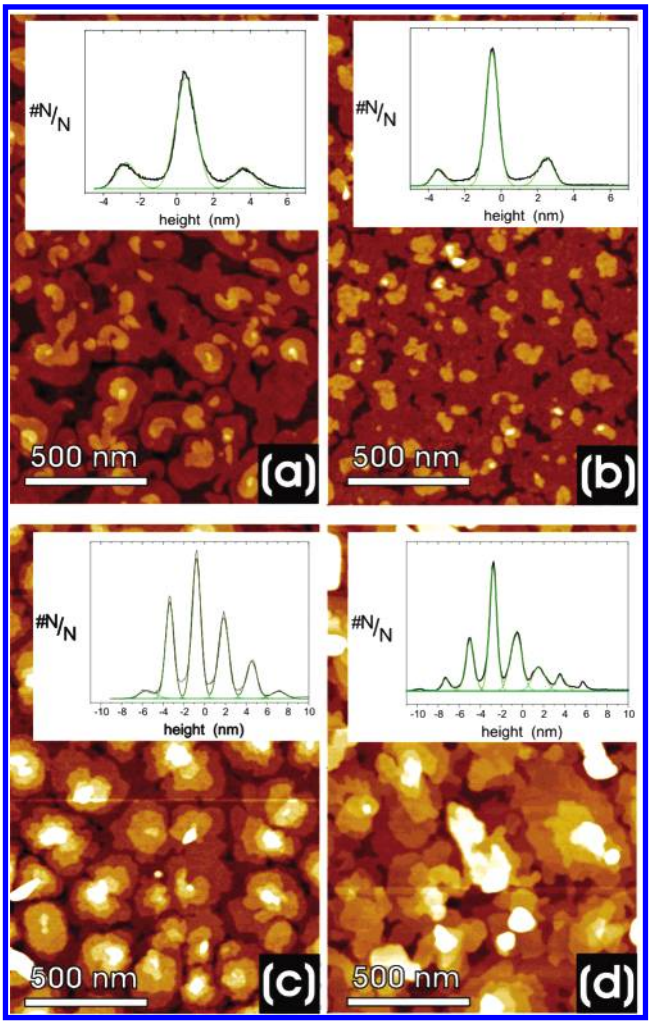

Figure 1. Tapping mode AFM images of co-deposited films 6T/DH6T films on SiO_2 of 20 nm nominal thickness: (a) 0% 6T; (b) 57% 6T; (c) 78% 6T; (d) 100% 6T. The insets show the height distribution of the images ($^{\#N}/_N$ relative number of pixels per height interval; the first peak corresponds to the bottom-most visible layer). The height scale is adjusted for maximum contrast.

momentum transfer (q_z) (see Figure 2a), which we assign to the (001) and (002) diffractions of a DH6T polymorph with a lattice spacing of $d = 3.64$ nm. This spacing is similar to the $d = 3.6$ nm spacing observed for small DH6T crystallites by Lovinger et al.[30] and to other reported d-values of DH6T on SiO_2 (3.55,[22] 3.54,[23] and 3.6 nm [30]). A film with 7% 6T exhibited two peaks at 0.170 and 0.339 $Å^{-1}$, which are assigned to (001) and (002) diffractions of a single material phase (which will be supported below by infrared spectroscopy results) with a lattice constant of $d = 3.71$ nm. A sample with 60% 6T exhibited peaks at 0.212 and 0.414 $Å^{-1}$, corresponding to $d = 2.96$ nm. The typical appearance of (001) and (002) diffractions is continued for a film with 79% 6T, resulting in $d = 2.7$ nm. However, pure 6T films exhibited polymorphism, as recognized by a broad (001) peak centered at 0.26 $Å^{-1}$ and a (002) peak at 0.52 $Å^{-1}$, corresponding to $d = 2.42$ nm (representing the known β-phase of 6T[31] with $d = 2.44$ nm). Sharper (001) and (002) peak components at 0.279 and 0.558 $Å^{-1}$ (yielding $d = 2.25$ nm) agree with the 6T γ-phase ($d = 2.24$ nm).[31]

The X-ray data of 6T/DH6T samples on Mylar substrates exhibited only (001) diffraction peaks, indicating lower order. This is in line with general expectations, since Mylar has a higher root-mean-square surface roughness (1 nm)[32] than silicon oxide (ca. 0.2 nm). Most notably, the resulting d values are

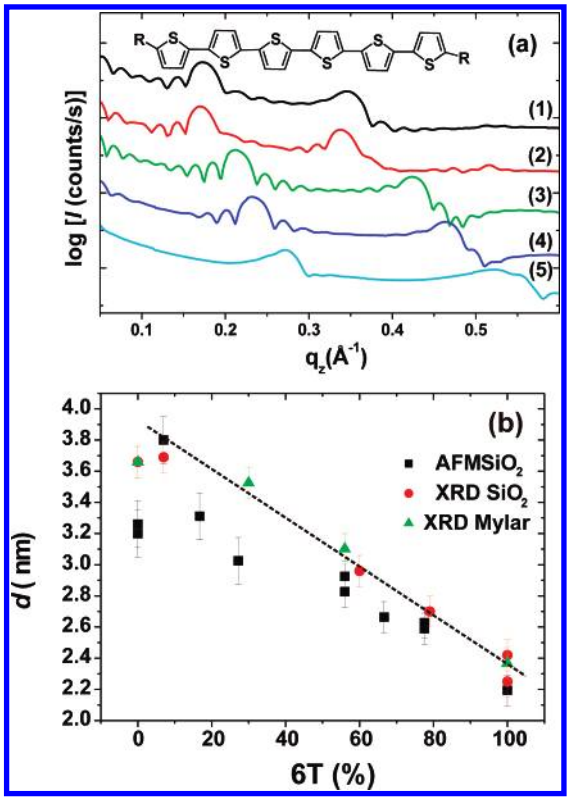

Figure 2. (a) X-ray diffraction spectra of co-deposited 6T/DH6T layers on SiO_2: (1) 0% 6T; (2) 7% 6T; (3) 60% 6T; (4) 79% 6T (5) 100% 6T. The spectra are shifted vertically for clarity. q_z is the vertical momentum transfer vector and log I is logarithm of the count rate. Inset: chemical structure of 6T (R = H) and DH6T (R = C_6H_{13}). (b) Interlayer distance d of 6T/DH6T co-deposited films on SiO_2 and Mylar measured by AFM and XRD as a function of 6T content. The dashed line is a guide for the eye of the linear dependence.

virtually identical to those obtained for silicon oxide substrates. All interlayer spacing values for the pair 6T/DH6T are summarized in Figure 2b, including values obtained independently from AFM measurements. We note that d values derived from AFM at DH6T proportions > 50% have a larger error due to the comparably small number of visible island steps. The dependence of d on the 6T/DH6T mixing ratio directly suggests a substrate-independent linear relation throughout the entire range investigated (except for pure DH6T, due to a different intralayer structure). These data alone provide already strong indications for an intercalation of 6T and DH6T.

More direct evidence for this intercalation was obtained from IR measurements (Figure 3a). For pure 6T, in the spectral region of 660−720 cm^{-1} we observed the $\gamma(C_\alpha-H)$ out of plane bending mode of the 6T terminal rings, which exhibited Davydov splitting into two peaks at 688 and 702 cm^{-1}.[33] On the other hand, 6T samples co-deposited with DH6T exhibited no clear-cut splitting and only one red-shifted asymmetric peak at 682 cm^{-1} was observed. DH6T showed no such peak since hexyl chains are attached to the α-position of the terminal rings. This means that DH6T intercalation of 21% was sufficient to change the unit cell of 6T molecules, thus subduing the Davydov splitting of pristine 6T. Furthermore, these spectra directly rule out the coexistence of DH6T and 6T crystallites (or layers) in mixed films. Changes of the in-plane structure (unit cell) of mixed 6T/DH6T samples compared to pure 6T samples were confirmed by preliminary grazing incidence X-ray diffraction experiments, which will be reported in detail elsewhere.

For DH6T, Garnier, et al.,[22] proposed that strong $\pi-\pi$ interactions between the rigid conjugated sexithiophene cores

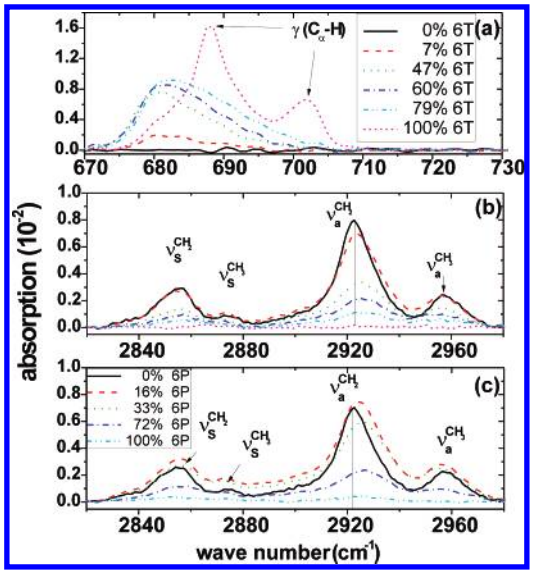

Figure 3. IR absorption spectra of co-deposited thin films on SiO_2: (a) $\gamma(C_\alpha-H)$ deformation region; (b) alkyl C−H stretching region of 6T/DH6T; (c) alkyl C−H stretching region of 6P/DH6T films.

and van der Waals interactions between the flexible alkyl chains leads to a separation of these subunits into alkyl and sexithiophene domains within one molecular layer.[30] The observed linear dependence of the interlayer spacing on the 6T/DH6T ratio (Figure 2b) can be related to this motif of intralayer phase separation. The observed changes in d could then be explained by two mechanisms: (i) The angle between hexyl chains and substrate, as well as the angle between sexithiophene-moieties and substrate, may depend on the intercalation level. (ii) The conformation of hexyl chains in co-deposited films changes, as free volume in the hexyl domain is created by replacing a DH6T molecule by 6T within one layer. As a consequence, hexyl domains should be less ordered in mixed films, e.g., by alterations of the tilt angle between conjugated core and hexyl chains or by some C−C bonds of the hexyls being in cis conformation (in densely packed pristine DH6T, hexyl chains are supposedly in the all-trans conformation[22]). While mechanism i is most likely the reason for the abrupt *increase* of d when going from pure DH6T to mixed films, we relate the gradual decrease of d for increasing 6T content to mechanism ii.

Support for this explanation is provided by IR data in the region of 2820−2980 cm^{-1} (Figure 3b), where C−H stretching vibrations of the hexyl groups of DH6T are located. We first discuss the pure DH6T (0% 6T) spectrum. The strongest peaks at 2855 and 2923 cm^{-1} can be assigned to the symmetric and antisymmetric C−H stretching bands of CH_2.[34] The small peaks at 2874 and 2958 cm^{-1} are due to the symmetric and antisymmetric C−H stretching band of the terminal methyl group of the DH6T hexyl chain.[34] The asymmetric CH_2 stretching peak exhibited a gradual blue shift of up to 3 cm^{-1} (for the 79% 6T co-deposited sample) for increasing 6T content in DH6T (Figure 3b). No energy shift was observed for the other alkyl stretching bands. Park et al.[34] reported that decreasing order and packing density of self-assembled monolayers of alkanethiols on Au led to a blue shift of the methyl C−H stretching band. Therefore, we conclude that in the co-deposited 6T/DH6T layers the order and packing density of the DH6T hexyl chains is lower compared to the pure DH6T films.

We now turn toward the material pair 6P/DH6T and will show that such co-deposited films exhibit the same behavior as 6T/DH6T films. Representative AFM images of co-deposited 6P/

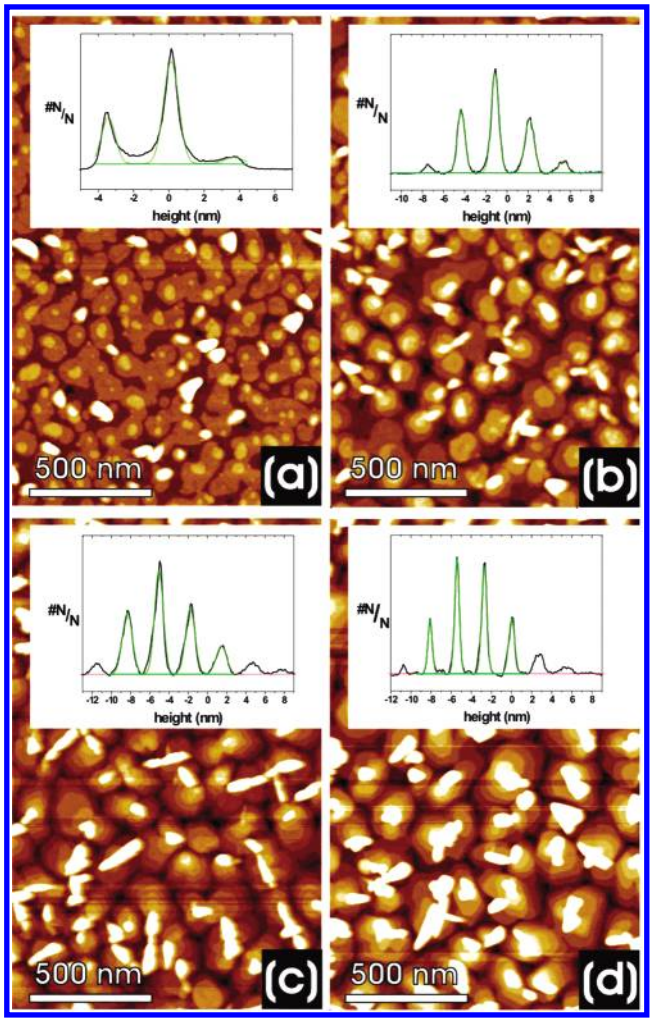

Figure 4. AFM height images of 20 nm thick co-deposited films of 6P and DH6T on SiO_2: (a) 18% 6P; (b) 44% 6P; (c) 73% 6P; (d) 100% 6P. The insets show the height distribution of the images after background subtraction. The height scale is adjusted for maximum contrast.

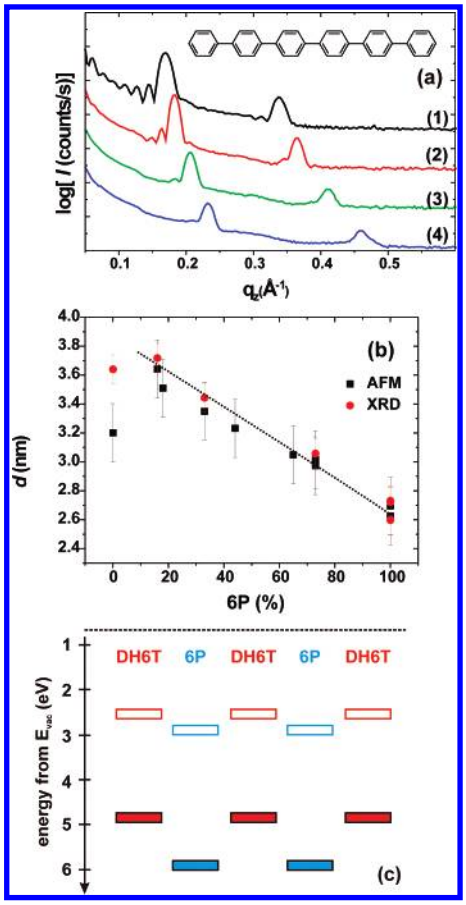

Figure 5. (a) X-ray diffraction of co-deposited 6P/DH6T layers on SiO_2: (1) 16% 6P; (2) 33% 6P; (3) 73% 6P; (4) 100% 6P. The spectra are shifted vertically for clarity. q_z is the vertical momentum transfer vector, and log I is the logarithm of the count rate. (b) Interlayer distance d of 6P/DH6T co-deposited films on SiO_2 measured by AFM and XRD as a function of 6P content. The dashed line is a guide for the eye of a linear dependence. (c) Schematic energy diagram within mixed 6P/DH6T samples, indicated by the positions (with respect to the vacuum level) of the highest occupied molecular orbitals (HOMOs, filled bars) and lowest unoccupied molecular orbitals (LUMOs, open bars).

DH6T films of 20 nm nominal thickness are depicted in Figure 4. The AFM micrograph of pure DH6T was depicted in Figure 1a. The morphology evolution for films with different molar ratios is similar for 6P/DH6T as for 6T/DH6T. For 18% 6P (Figure 4a), smaller islands were observed compared to pure DH6T. The 44% 6P film (Figure 4b) exhibited a more granular appearance with still rather round island shapes. The morphology of the 73% 6T film (Figure 4c) displays more pyramidlike islands and with more apparent height levels of individual terraces. Pure 6P (Figure 4d) showed the characteristic pyramidlike morphology with also seven exposed molecular layers, however, with increased island density and rather smooth island edges compared to pure 6T. Thus, the surface morphology of mixed 6P/DH6T films also changed gradually depending on the ratio between DH6T and 6P. The 16% 6P sample showed (001) and (002) reflections ($q_z = 0.169$ and 0.338 Å^{-1}, respectively; see Figure 5a) corresponding to $d = 3.72$ nm. Similar assignments yielded $d = 3.44$ nm for 33% 6P and $d = 3.06$ nm for 73% 6P. The pure 6P film showed two slightly asymmetric (001) and (002) peak series, corresponding to the coexistence of the γ-phase[35] ($d = 2.72$ nm) and a small fraction of the β-phase[35] ($d = 2.60$ nm). The interlayer spacings measured by AFM are included in the compilation of X-ray data as function of 6P content in Figure 5b. The intralayer spacing d for 6P/DH6T films thus shows the same linear dependence on 6P content as the 6T/DH6T films (with the dependence on 6T content).

The IR data in the region of 2820−2980 cm^{-1} (Figure 3c), where C−H stretching vibrations of the hexyl group of DH6T are located, show exactly the same trend as those for 6T/DH6T samples. The asymmetric CH_2 stretching peak gradually blue shifts by up to 3 cm^{-1} (for 72% 6P) for increasing 6P content in DH6T. Consequently, we conclude an intercalation of 6P and DH6T, facilitated by the flexibility of DH6T hexyl chains, in full analogy to the above discussion of 6T/DH6T samples (cf. schematic of both structures shown in Figure 6). In general, it thus appears that the strong $\pi-\pi$-interactions between even dissimilar conjugated cores are responsible for the observed intercalation behavior. Phase separation, instead, would result in the mixture of inhomogeneous layer thickness (i.e., alkylated versus nonalkylated domains) within one nominal layer, which seems energetically unfavorable, in particular in three-dimensional growth. A systematic change in the tilt angle of the molecules for different film compositions as reason for the observed d variation can be ruled out as this would require two different tilt angles for DH6T and 6T within a sample, which would lead to phase separation. The opposite was observed.

Notably, the mixed 6P/DH6T samples exhibit layered structures, where the energy gap *within* a two-dimensional layer varies by ca. 0.7 eV (i.e., from 3.0 eV for 6P to 2.3 eV for

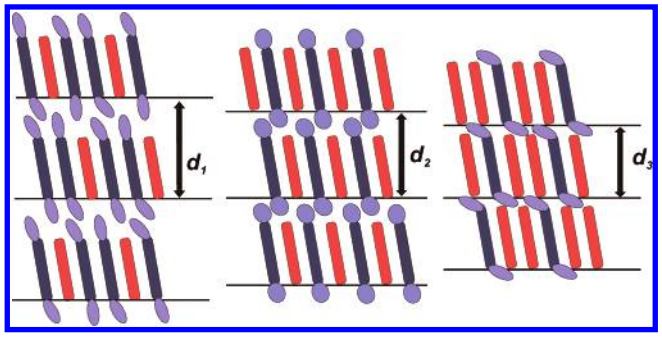

Figure 6. Schematic molecular arrangements for intercalated films, indicating different interlayer spacings $d_1 > d_2 > d_3$.

DH6T) on a molecular length scale, as schematically shown in Figure 5c. For the future, it should be interesting to investigate the influence of this energy modulation on the dynamics of charge carriers and excitons, as the energy positions for electrons and holes are highly defined. An additional feature of our structures is that the 2D semiconducting (conjugated) layers are vertically separated by insulating alkyl chains (see schematic in Figure 6), thus combining two essential electronic functionalities on the nanometer scale in a tunable (via *d*) and ordered way.

Conclusion

In conclusion, we prepared vacuum co-deposited thin films of the material pairs 6T/DH6T and 6P/DH6T, with varying molecular ratios. AFM and X-ray measurements showed that the films have a layered structure and that the interlayer distance *d* depends linearly on the 6T/DH6T ratio. This dependence was observed for two very different substrates materials, i.e., inorganic SiO_2 (low surface roughness) and the polymer Mylar (high surface roughness), indicating that it is not particular to the substrate. The *d* dependence is attributed to the intercalation of 6T and DH6T within layers, due to the strong $\pi-\pi$ interaction of the conjugated molecular cores, and the flexibility of DH6T hexyl chains, as evidenced by IR investigations. The same intercalation mechanism leads also to a linear *d* dependence for the 6P/DH6T pair, where *dissimilar* conjugated cores are forming mixed layers. Thus, vacuum co-deposition of a rigid conjugated molecule with an alkylated rodlike molecule should be a practical method to fabricate mixed layers containing two conjugated moieties with vastly different electronic properties and at the same time to tune interlayer distances with sub-nanometer precision. This type of self-assembly of organic molecules on a substrate from the vapor phase will enable detailed investigations of intermolecular coupling between conjugated layer stacks, separated by controlled insulating layers, in a simple manner.

Acknowledgment. DH6T was kindly provided by H. C. Starck GmbH & Co. KG and Mylar substrates by A. Bonfiglio and P. Cosseddu (University of Cagliari). The authors thank J. Pflaum and S. Hirschmann (Universität Stuttgart) for purifying 6T. This work was supported by Grant Sfb448 (DFG). N.K. acknowledges financial support by the Emmy Noether-Program (DFG). B.N. acknowledges financial support from Grant SP 1121 (DFG) and from CeNS.

References and Notes

(1) Barth, J. V.; Costantini, G.; Kern, K. *Nature* **2005**, *437*, 671.
(2) Kuhn, H.; Mobius, D. *Angew. Chem., Int. Ed. Engl.* **1971**, *10*, 620.
(3) Maoz, R.; Matlis, S.; DiMasi, E.; Ocko, B. M.; Sagiv, J. *Nature* **1996**, *384*, 150.
(4) Samori, P.; Francke, V.; Müllen, K.; Rabe, J. P. *Chem.−Eur. J.* **1999**, *5*, 2312.
(5) Schmidt-Mende, L.; Fechtenkötter, A.; Müllen, K.; Moons, E.; Friend, R. H.; MacKenzie, J. D. *Science* **2001**, *293*, 1119.
(6) Cacialli, F.; Wilson, J. S.; Michels, J. J.; Daniel, C.; Silva, C.; Friend, R. H.; Severin, N.; Samori, P.; Rabe, J. P.; O'Connell, M. J.; Taylor, P. N.; Anderson, H. L. *Nature Mater.* **2002**, *1*, 160.
(7) Kato, T. *Science* **2002**, *295*, 2414.
(8) Leclere, P.; Surin, M.; Viville, P.; Lazzaroni, R.; Kilbinger, A. F. M.; Henze, O.; Feast, W. J.; Cavallini, M.; Biscarini, F.; Schenning, A. P. H. J.; Meijer, E. W. *Chem. Mater.* **2004**, *16*, 4452.
(9) Jäckel, F.; Watson, M. D.; Müllen, K.; Rabe, J. P. *Phys. Rev. Lett.* **2004**, *92*, 188303.
(10) Samori, P.; Yin, X. M.; Tchebotareva, N.; Wang, Z. H.; Pakula, T.; Jäckel, F.; Watson, M. D.; Venturini, A.; Müllen, K.; Rabe, J. P. *J. Am. Chem. Soc.* **2004**, *126*, 3567.
(11) Yokoyama, T.; Yokoyama, S.; Kamikado, T.; Okuno, Y.; Mashiko, S. *Nature* **2001**, *413*, 619.
(12) Mena-Osteritz, E. *Adv. Mater.* **2002**, *14*, 609.
(13) Rand, B. P.; Xue, J. G.; Uchida, S.; Forrest, S. R. *J. Appl. Phys.* **2005**, *98*, 124902.
(14) Xue, J. G.; Rand, B. P.; Uchida, S.; Forrest, S. R. *J. Appl. Phys.* **2005**, *98*, 124903.
(15) Yang, F.; Shtein, M.; Forrest, S. R. *J. Appl. Phys.* **2005**, *98*, 014906.
(16) Han, E. M.; Do, L. M.; Yamamoto, N.; Fujihira, M. *Thin Solid Films* **1996**, *273*, 202.
(17) Peumans, P.; Uchida, S.; Forrest, S. R. *Nature* **2003**, *425*, 158.
(18) Porzio, W.; Giovanella, U.; Pasini, M.; Botta, C.; Destri, S.; Provasi, C. *Thin Solid Films* **2004**, *466*, 231.
(19) Salzmann, I.; Opitz, R.; Rogaschewski, S.; Rabe, J. P.; Nickel, B.; Koch, N. *Phys. Rev. B* **2007**, *75*, 174108.
(20) Garnier, F.; Horowitz, G.; Peng, X. H.; Fichou, D. *Adv. Mater.* **1990**, *2*, 592.
(21) Fichou, D. *J. Mater. Chem.* **2000**, *10*, 571.
(22) Garnier, F.; Yassar, A.; Hajlaoui, R.; Horowitz, G.; Deloffre, F.; Servet, B.; Ries, S.; Alnot, P. J. *Am. Chem. Soc.* **1993**, *115*, 8716.
(23) Facchetti, A.; Mushrush, M.; Yoon, M. H.; Hutchison, G. R.; Ratner, M. A.; Marks, T. J. *J. Am. Chem. Soc.* **2004**, *126*, 13859.
(24) Gundlach, D. J.; Lin, Y. Y.; Jackson, T. N.; Schlom, D. G. *Appl. Phys. Lett.* **1997**, *71*, 3853.
(25) Tasch, S.; Brandstatter, C.; Meghdadi, F.; Leising, G.; Froyer, G.; Athouel, L. *Adv. Mater.* **1997**, *9*, 33.
(26) Resel, R.; Koch, N.; Meghdadi, F.; Leising, G.; Unzog, W.; Reichmann, K. *Thin Solid Films* **1997**, *305*, 232.
(27) Servet, B.; Ries, S.; Trotel, M.; Alnot, P.; Horowitz, G.; Garnier, F. *Adv. Mater.* **1993**, *5*, 461.
(28) Cosseddu, P.; Bonfiglio, A. *Appl. Phys. Lett.* **2006**, *88*, 023506.
(29) Bonfiglio, A.; Mameli, F.; Sanna, O. *Appl. Phys. Lett.* **2003**, *82*, 3550.
(30) Lovinger, A. J.; Katz, H. E.; Dodabalapur, A. *Chem. Mater.* **1998**, *10*, 3275.
(31) Servet, B.; Horowitz, G.; Ries, S.; Lagorsse, O.; Alnot, P.; Yassar, A.; Deloffre, F.; Srivastava, P.; Hajlaoui, R.; Lang, P.; Garnier, F. *Chem. Mater.* **1998**, *6*, 1809 .
(32) Milita, S.; Santato, C.; Cicoira, F. *Appl. Surf. Sci.* **2006**, *252*, 8022.
(33) Kramer, M.; Hoffman, V. *Opt. Mater.* **1998**, *9*, 65.
(34) Park, J. S.; Vo, A. N.; Barriet, D.; Shon, Y. S.; Lee, T. R. *Langmuir* **2005**, *21*, 2902.
(35) Resel, R.; Koch, N.; Meghdadi, F.; Leising, G.; Athouel, L.; Froyer, G.; Hofer, F. *Cryst. Res. Technol.* **2001**, *36*, 47.